3 Particle Physics at DESY/HERA (H1)

J. Becker, Ilaria Foresti, N. Keller, H. Klehr, J. Kroseberg (until May 2003),
L. Lindfeld, Katharina Müller, P. Robmann, S. Schmitt, C. Schmitz, U. Straumann,
P. Truöl, M. Urban, Nicole Werner and Stefania Xella Hansen

in collaboration with:
S. Baumgartner, N. Berger, W. Erdmann, C. Grab, B. List, S. Mangano, D. Meer, A. Schöning and R. Weber, Institut für Teilchenphysik der ETH, Zürich; S. Egli, R. Eichler, K. Gabathuler, M. Hildebrandt, and R. Horisberger, Paul–Scherrer–Institut, Villigen, and 34 institutes outside Switzerland

(**H1**–Collaboration)

3.1 Electron–proton collisions at a centre of mass energy up to 320 GeV: overall status of the project

The analysis of the data taken in 1999/2000 ($\mathcal{L} = 91$ pb^{-1}), combined in some cases with the pre–1999 data ($\mathcal{L} = 50$ pb^{-1}) continued vigorously leading to 14 publications ([1]-[14]) and 27 papers contributed to the 2003 high–energy physics conferences [15] ([16]-[42]), addressing the following subjects:

- Neutral and charged electroweak current cross sections, proton structure functions and parton densities (extensions into lower and higher Q^2 regimes, use of QED–Compton scattering events) [3; 16; 17; 18; 44; 45];
- Search for states and interactions outside the Standard Model: unexpected event topologies [2; 41], compositeness [4], squarks [12], gravitinos [42], leptoquarks [39], single top [7], charged Higgs [40], anomalous lepton pairs [6; 8], magnetic monopoles [40] and heavy stable charged particles [13];
- Photo– and electro–production of di– and multi–jets [2; 9; 10; 24; 25; 27];
- Photo– and electro–production of exclusive final states: π^0 [14], ρ [32], J/Ψ [5; 34], antideuterons [13];
- Production of open charm and beauty: anti–charmed baryon state [11], inclusive charm [20; 21; 22; 23], inclusive beauty [26];
- Diffractively produced final states: inclusive [28; 29; 30; 31; 36], π^0 [14], jets [27], ρ, $f_0(980)$, and $f_2(1270)$ [32], J/Ψ [5; 34], high p_t photons [35];
- Photon structure [19] and deeply virtual Compton scattering [37].

3.2 Status of the HERA accelerator

Since the end of the HERA shutdown in September 2003 the vacuum and background situation has significantly improved. This was achieved by the installation of an additional ion getter pump, in-

creased pumping power and a lead shield around the beam pipe for better synchrotron radiation protection.

From January to end of April 2004 HERA–II has continuously delivered data up to an integrated luminosity of 37.2 pb^{-1}. The produced integrated luminosity as a function of time is shown in Fig. 3.1 together with the luminosity recorded with H1. The slope of the curve for 2004 is similar to that in the year 2000 with higher specific luminosity but lower duty cycle. The maximum instantaneous luminosity achieved up to end of April was $3.5 \cdot 10^{31}$ cm^2/s. Both beam intensities and specific luminosity have thus reached the HERA-II upgrade design values. However, there is still room for improvements in the reliability of various technical elements of the accelerators, in order to increase the duty cycle of the machine.

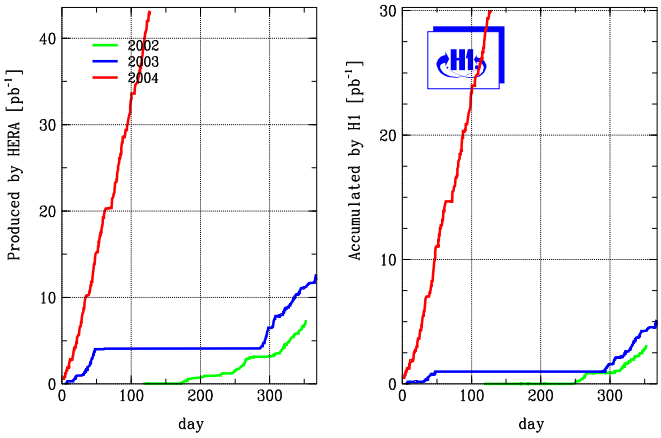

Figure 3.1:
Left: integrated luminosity produced by HERA–II as a function of time.
Right: integrated luminosity accumulated by H1 as a function of time.

3.3 Commissioning and first operation of the new z–vertex trigger

3.3.1 Repair of the CIP2k frontend electronics

In summer 2003 we had the chance to access the front–end electronics of the CIP2k chamber and repair some broken channels. After removing the SpaCal calorimeter and disconnecting the beam–pipe the CIP2k chamber was retracted by about 50 cm and the front–end electronics was removed and repaired. Boards which could not be repaired were replaced. The new/repaired electronics was tested using a three–step procedure:

- Check the response of each single channel with a special test board.
- Connecting to the standard readout and slow control system and doing pedestal and noise runs.
- Connecting each board to the standard readout again after attaching it to the chamber.

All 40 boards passed these tests and the chamber was put back in place. A second cooling ring was installed, and the heat conduction improved, in order to prevent the front–end electronics from over–heating.

3.3.2 Performance of the new z–vertex trigger

Since the synchrotron radiation background increased with the upgrade the quality of the vacuum in the beam pipe degraded, in particular in the backward region (incoming proton direction) of the

detector. Thus, background from collisions between protons and rest gas nuclei increased. These are observed as hadronic showers coming from the backward direction.

To cope with this higher background rate a dead time free trigger system was developed for the H1 experiment that is able to distinguish between beam background events and true ep interactions. This CIP2k z–vertex trigger recognises particle tracks, calculates a histogram of their origins along the beam axis and derives a trigger decision by evaluating this histogram.

The system has been described in detail in earlier annual reports. It is based on a set of five cylindrical multi–wire proportional chambers (CIP2k) of 2 m length and 40 cm diameter, with a cathode readout granularity of 16 in azimuth angle ϕ and 120 along the beam axis. A total of about 8,500 channels are amplified, digitised and synchronised to the accelerator clock (10.4 MHz) immediately on the detector. The resulting binary data is optically transmitted to the trigger logic in the counting house.

The pipelined H1 trigger system requires a dead time free calculation of the trigger response, which has to be available 2.3 μs after the event occurred. We use large FPGAs (APEX20k400) both for the trigger calculation and for the storage of the complete binary data for later readout by the data acquisition system. Due to their embedded memory these FPGAs are very well suited for the implementation of ring buffers with 32 bunch crossings for pipelined data acquisition storage. The complete trigger and storage functionality for one of the 16 ϕ–sectors fits into two FPGAs. The trigger calculation runs synchronously with the accelerator clock and its latency amounts to 960 ns.
Tests with minimum ionising particles have been performed after the repair efforts in summer 2003 using cosmic ray muons in order to check the performance of the system. To ensure the correct timing of the data in the pipelines the trigger decision derived by the trigger system was compared to the results of a complete software simulation of the trigger system, based on the readout of the corresponding bunch crossing. Furthermore correlations between tracks recognised in the drift chamber of the H1 detector and tracks triggered by the CIP2k system have been studied. The deviation of the vertex position found by the CIP2k trigger from the vertex position reconstructed offline is shown in Fig. 3.2. The position resolution is found to be 16.7 cm in agreement with expectations. The single track efficiency in the trigger is better than 95%..

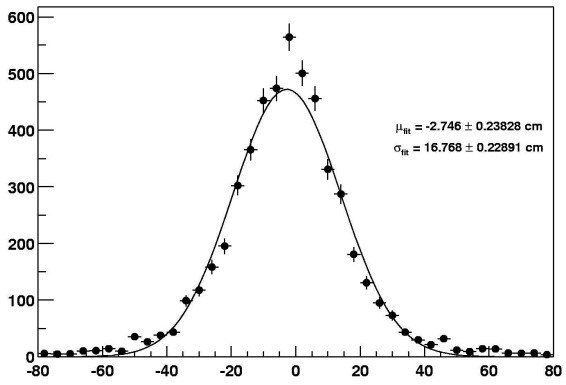

Figure 3.2: *Deviation of the vertex position found by the CIP2k trigger from the vertex position reconstructed offline.*

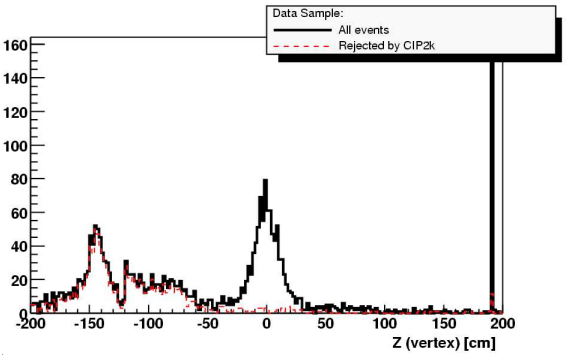

Figure 3.3: *Rejection power of the CIP2k system. Shown is the z–vertex position of all events including the background coming from the backward direction, i.e. negative z values (full line) and the events which are rejected by the CIP2k trigger (dashed line).*

First events taken in ep collisions, provided by HERA–II since October 2003, were used to tune details of the behaviour of the CIP2k trigger. An excellent rejection power against proton beam background of the CIP2k trigger system was established as can be seen in Fig. 3.3. Presently the

CIP2k trigger is routinely used to reject background events and to provide precise timing information in most H1 physics trigger combinations. Further improvements of the performance for triggering selected physics channels are ongoing. This new trigger system was the thesis project of Max Urban who received his Ph.D. recently [43].

3.3.3 Reimplementation of the old z–vertex trigger

In addition to the upgrade of the z–vertex trigger we reimplemented the old readout and z–vertex trigger system parallel to the new system. The new CIP2k trigger fills a z–vertex histogram by a projective geometry of five readout layers at small radii, whereas the old system used the two layers of the two separated chambers CIP and COP (central outer proportional chamber). Due to the roughly 50 cm long lever arm between CIP and COP, the old z–vertex histogram has a better resolution in z compared to the new histogram. Moreover, the longer lever arm allows to cut off very low momentum tracks from the trigger. For instance, heavy flavour triggers use the track multiplicity given by the old z–vertex trigger.

The interesting and rare high p_t (Sec. 3.5.3) and charged current (Sec. 3.6.1) events with an undetectable neutrino in the final state rely on an efficient triggering of missing transverse energy in the detector. This can be improved by the combination of information delivered by the old z–vertex trigger and by the liquid argon calorimeter using *Big Rays* pointing from tracks of charged particles to corresponding areas of the calorimeter. The sensitivity of the calorimeter and therefore the efficiency for triggering on events with small energy deposits is limited by the noise in the calorimeter cells. The coincidence of *Big Rays* pointing to energy depositions in the calorimeter allows to lower the threshold values locally and thus leads to higher trigger efficiencies for events with low tranverse energy. Both, the old z–vertex trigger and the *Big Ray* system, were originally built by our group (theses of S. Eichenberger (1993) and H. P. Beck (1996)).

In order to feed the readout of the old CIP with signals from the CIP2k a hardware interface was realised in 2003. The signals of the innermost two layers of the new CIP2k are de–multiplexed, shaped and logically combined to enter the old receiver cards. After the signals are matched in time with the COP signals the old z–vertex trigger system delivers the trigger elements to the first trigger level as it was before 2001. The system is still being optimised with Linus Lindfeld acting as the person mainly responsible.

3.3.4 Steering of the CIP2k

During the 2003 summer shutdown and the successive test operation period, the slow control software for the CIP2k was implemented in PVSS (Prozess Visualisierungs– und Steuerungs–Software). PVSS is a software package allowing the efficient development of control software for complex technical systems. It features a variety of control features like alarms, data logging, redundancy, automatic reporting and others. The system was chosen by the H1DCM (H1 detector control management) project group as the standard slow control software for H1, it is also foreseen to be used in most LHC projects.

The high voltage control was unified for all tracking detectors by the H1DCM group using PVSS. For all other control tasks of the CIP2k as are the data acquisition system, the trigger, the front–end and the temperature monitoring a PVSS application was developed by Hannes Klehr. About 60 distinct parameters for multiple hardware components are monitored and adjusted. The graphical user interface allows quick access to all parameters. Procedures for standard tasks, e.g. programming the front–end

electronics have been implemented. During the first data taking periods with cosmic ray muons and with electron–proton collisions the user friendly interface helped optimising the parameters quickly for an efficient operation. The interface is documented in a user manual.

3.4 Activities of the Polarimeter group

The Polarimeter group at DESY consists of members of H1, HERMES, ZEUS and DESY. The group is responsible for the operation of the HERA–II electron beam polarimeters (transverse and longitudinal polarimeter, TPOL and LPOL). Stefan Schmitt is acting as the speaker of this group. Apart from coordinating the group activities the main focus of his work in the polarimeter group [46] is the operation of the TPOL and the analysis of the TPOL data. The polarimeters are based on Compton scattering of laser light and the electron beam. The scattered Compton photons are detected in a small calorimeter.

The TPOL is located in the HERA tunnel far from spin rotators, where the lepton polarisation is transverse. It measures the polarisation by detecting the energy and vertical position of single Compton photons at a rate of 50–100 kHz. The laser light is coming from a 10 W cw laser. The calorimeter is divided into two halves to give sensitivity to the spatial coordinate. The lepton polarisation is determined from the asymmetry in the spatial coordinate when comparing the cross section for left– and right–circular polarised laser light.

The LPOL is located in the HERA tunnel near the HERMES experiment, between a pair of spin rotators where the lepton polarisation is longitudinal. The polarimeter measures the polarisation by detecting the mean energy of about 1000 Compton photons, scattered from a single bunch using a high–power pulsed laser with a repetition rate of about 100 Hz. The energy of the photons is averaged because their showers overlap in the same calorimeter. The lepton polarisation is determined by the asymmetry in the mean energy when comparing left– and right–circular polarised laser light.

In the summer shutdown 2003 a Fabry–Perot cavity was installed near the existing LPOL interaction point. It is fed by a 1W cw laser. The power stored inside the cavity can be amplified by a factor of 5000. Using the high photon density inside the cavity, it is possible to produce Compton photons at a rate of 10 MHz (the HERA bunch crossing rate). By recording the energy spectra of these photons the single differential cross section is accessible and the beam polarisation can be measured with ultimate precision. The LPOL cavity is still in the phase of commissioning.

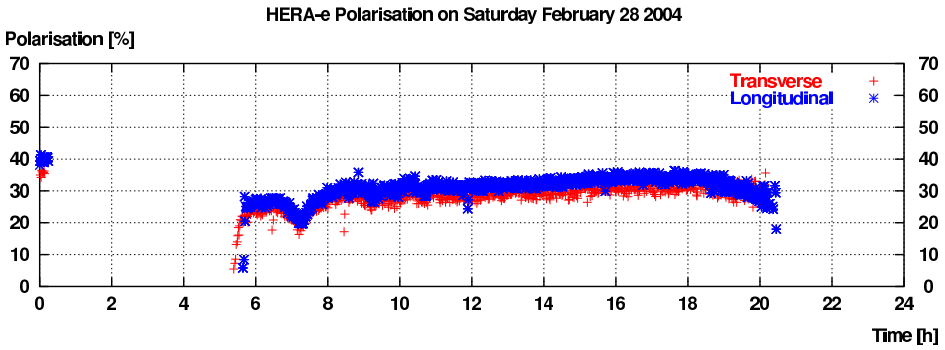

Figure 3.4: *Lepton polarisation measured by LPOL and TPOL during a typical HERA fill.*

During 2003 the two lepton polarimeters were fully operational whenever HERA was running. Figure

3.4 shows the lepton polarisation measured by LPOL and TPOL during a typical HERA fill. Typical polarisation values reached by HERA are up to 40% during luminosity operation. The polarisation is subject to constant tuning by the HERA operators. The expected maximum polarisation with three spin rotators is up to 60%. The main challenge for the Polarimeter group is to get a correct calibration of the absolute scale of both polarimeters.

3.5 Results from recent analyses

3.5.1 Evidence for a new anti–charmed baryon state

We have observed a narrow resonance in the $D^{*-}p$ and $D^{*+}\bar{p}$ invariant mass combinations in the analysis of deep inelastic scattering events ($1 < Q^2 < 100$ GeV^2) recorded between 1996 and 2000 ($\mathcal{L} = 75$ pb^{-1}, 88 % e^+ and 12 % e^-) [11]. The resonance has a mass of $(3099 \pm 3$ (stat.) ± 5 (syst.)) MeV and a measured Gaussian width of $(12 \pm 3$ (stat.)) MeV, compatible with the experimental resolution. We interprete this new state as an anti–charmed baryon with a minimal constituent quark composition of $uudd\bar{c}$, together with its charge conjugate.

The analysis was motivated by the fact that several experiments have recently reported the observation of a narrow resonance with a mass near 1540 MeV, decaying to K^+n or $K^0_s p$ (see [11] for references). The latter state has both baryon number and strangeness of $B = S = 1$, such that its minimal composition in the constituent quark model is $uudd\bar{s}$ (*pentaquark* Θ^+). Various models have been put forward to explain the nature of these states and the structure of the multiplet that contains them, many of which naturally also call for extensions into the charm sector.

Through the boson–gluon fusion mechanism states with open and hidden charm are produced copiously and the most efficient way to tag them is via the detection of the $D^{*\pm}$ decay chains [47]

$$D^{*-} \to \bar{D}^0\pi^-_s \to K^+\pi^-\pi^-_s,$$
$$D^{*+} \to D^0\pi^+_s \to K^-\pi^+\pi^+_s\,.$$

This signal is easily detectable in the distribution of the mass difference variable $\Delta M_{D^*} = m(K\pi\pi_s) - m(K\pi)$ (see Fig. 3.5). The resonance is observed when combining $D^{*-} \to \bar{D}^0\pi^-_s \to K^+\pi^-\pi^-_s$ candidates with protons and $D^{*+} \to D^0\pi^+_s \to K^-\pi^+\pi^+_s$ candidates with anti–protons (see Fig. 3.6). The resonance is also observed in an

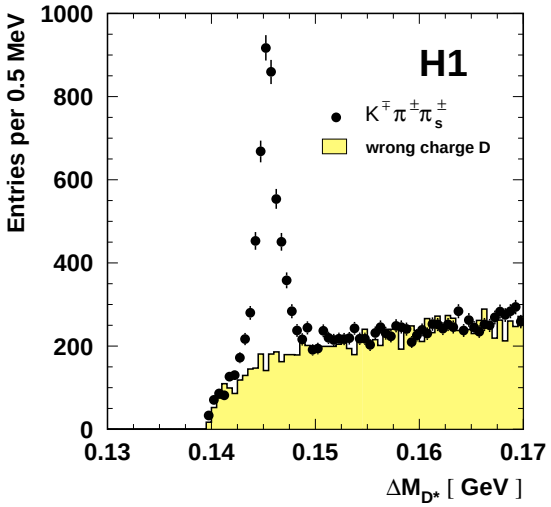

Figure 3.5: *ΔM^*_D mass distribution for $K^{\mp}\pi^{\pm}\pi^{\pm}_s$ combinations. Wrong charge combinations refer to those events where K and π have the same charge and invariant mass near $m(D^0)$.*

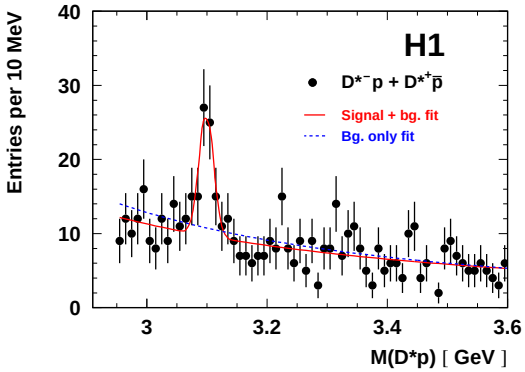

Figure 3.6: *$M(D^*p)$ mass distribution from opposite charge D^*p combinations compared with the results of a fit in which both signal and background components are included (solid line) and with the result of a fit in which only the background is included (dashed line).*

independent photoproduction data sample. The identification of protons and anti–protons is aided by the specific energy loss derived from the mean of the inverse square root of the charge collected by all wires of the central drift chamber showing a signal ($\sigma(dE/dx)/(dE/dx) \approx 8\%$). Approximately half of the events in the narrow peak observed for the opposite–charge combinations at $M(D^*p)$ near 3100 MeV arise from either protons or anti–protons. The distribution for the same–charge combinations $K^-\pi^+\pi_s^+p$ and $K^+\pi^-\pi_s^-\bar{p}$ does not show such a signal.

Fits to the $M(D^*p)$ distribution (opposite charge combinations) have been carried out to evaluate the peak position, width and statistical significance. Assuming the measured width to be dominated by the experimental resolution, a Gaussian distribution is used for the signal, with the peak position, the width and the normalisation as free parameters. The background is parameterised with a power law. The results quoted above are derived from a fit in the range $2950 < M(D^*p) < 3600$ MeV, and are compared with the data in Fig. 3.6. The signal contains 50.6 ± 11.2 events, corresponding to roughly 1 % of the total D^* production rate in the kinematic region studied. The systematic uncertainty on the mass of the peak is 5 MeV, estimated from the reconstructed masses of known states, such as the J/Ψ. The probability that the background distribution fluctuates to at least produce the signal has been evaluated to 4×10^{-8}. To arrive at this result the observed number of events was compared with background estimates for a window spanning $3075 < M(D^*p) < 3123$ MeV, corresponding to $\pm 2\sigma$ around the peak position. The total number of events in this interval is 95. The background contribution estimated using the fit described above is 45.0 ± 2.8 (stat.) events. A consistent number of background events is obtained with a parameterisation using a two–component background model. This model uses wrong charge D ($K^\pm\pi^\pm$) combinations to describe non–charm related background, and Monte Carlo generated events for real D^* background. In our publication several tests are described which concern the particle identification, the possibility for kinematical reflections faking such a signal as well as the consistency of different subsets of the data. The region of $M(D^*p)$ in which the signal is observed contains a richer yield of D^* mesons and exhibits a harder proton candidate momentum distribution than it is the case for side bands in $M(D^*p)$.

3.5.2 Inclusive Beauty production

Muons with a relatively large transverse momentum with respect to the axis of the hadronic jet to which they belong, a distinguishable secondary decay vertex or at least tracks with a large distance of closest approach to the primary vertex in the event are the signatures which are exploited to measure beauty production. The latter technique based on the longer lifetime of the hadrons with open beauty was pioneered in the thesis of J. Kroseberg [49] for the pre–1997 data. Now two analyses are available which extend these methods to the data taken in 1999/2000. The first comprises an integrated luminosity of $\mathcal{L} = 50$ pb^{-1} and contains events with at least one jet with a transverse momentum $p_t^{jet} > 6$ GeV and pseudo–rapidity $|\eta^{jet}| < 2.5$ and a muon associated to this jet with $p_t^\mu > 2.5$ GeV and $-0.75 < \eta^\mu < 1.15$. Differential jet–muon cross sections are evaluated for the first time, namely in the region of photon virtuality $2 < Q^2 < 100$ GeV^2 and inelasticity $0.1 < y < 0.7$. Figures 3.7 and 3.8 illustrate the separation technique and give some of the results. Within the albeit large statistical and systematic

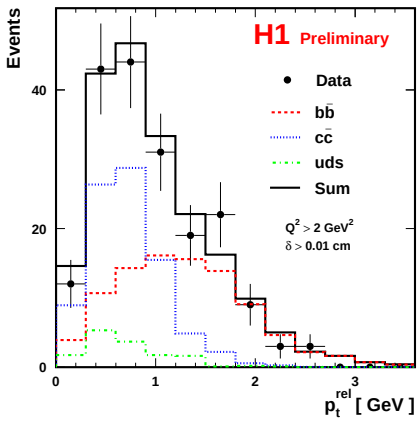

Figure 3.7: *Transverse muon momentum $p_t^{rel,\mu}$ distribution for events with impact parameters $\delta > 100$ μm with the light, charm and beauty quark contributions indicated.*

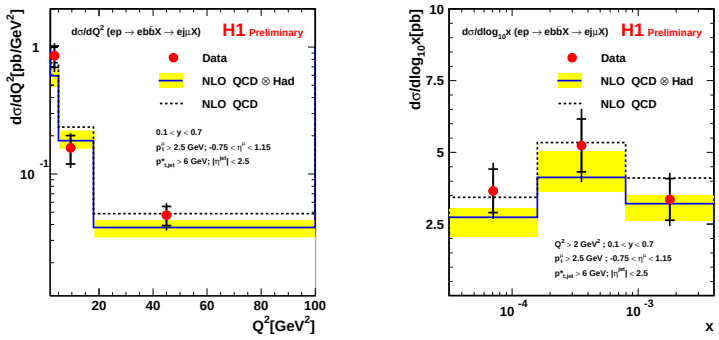

Figure 3.8: *Differential dijet muon production cross sections $d\sigma/dQ^2$ and $d\sigma/dx$ $(ep \rightarrow eb\bar{b}X \rightarrow ej\mu X)$. The inner error bars show the statistical error, the outer include the systematic uncertainty added in quadrature. The results for next–to–leading order perturbative QCD calculation [53] at parton (dashed line) and hadron (solid line) level are also shown.*

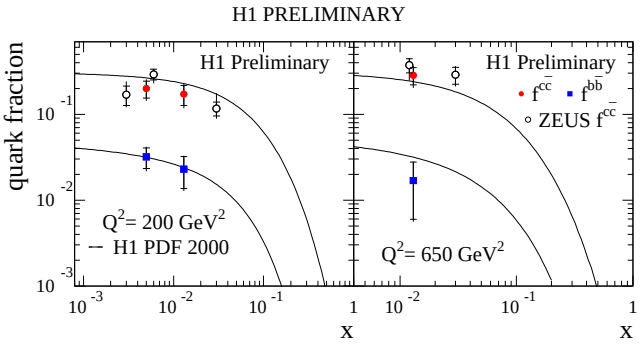

Figure 3.9: *The ratio $f^{c\bar{c}} = F_2^{c\bar{c}}/F_2$ and $f^{b\bar{b}} = F_2^{b\bar{b}}/F_2$ as a function of Bjorken–x for two different values of Q^2. The solid lines represent predictions derived from a next–to–leading order QCD fit to inclusive H1 data [3].*

uncertainties the agreement with next–to–leading order perturbative QCD predictions [53] is satisfactory. The second analysis concentrates on high momentum transfer events $Q^2 > 150$ GeV^2 and inelasticity $0.1 < y < 0.7$ and uses solely the distance of closest approach to the primary vertex reconstructed from tracks observed in the silicon vertex detector to enhance the beauty fraction. Beauty, charm and light quark contributions are separated by fitting the observed distributions to Monte Carlo simulations. The data could be divided into three bins in x and Q^2. The results, expressed as the ratio $f^{c\bar{c}} = F_2^{c\bar{c}}/F_2$ and $f^{b\bar{b}} = F_2^{b\bar{b}}/F_2$ are given in Fig. 3.9. Again the results are in satisfactory agreement with theoretical expectations but also (for charm) with ZEUS results.

3.5.3 High p_t data from HERA II

With the HERA accelerator complex finally reaching its post–upgrade expectation it is gratifying to see the first results arriving from data taken early this year. An analysis based on an integrated luminosity of $\mathcal{L} = 17$ pb^{-1} of high transverse momentum events including isolated leptons, multi–electrons and large missing transverse momentum has been prepared for the spring conferences in 2004 [48]. The analysis makes use of the techniques described in references [1] and [6]. For example ten di–electron and two tri–electron events are observed, compared to the Standard Model expectation of 15.8 ± 1.7 and 3.0 ± 0.4, respectively. Two electron events with missing transverse momentum above 25 GeV are observed while the Standard Model (dominated by real W–boson production) predicts 0.3 events. One of these events is shown in Fig. 3.10.

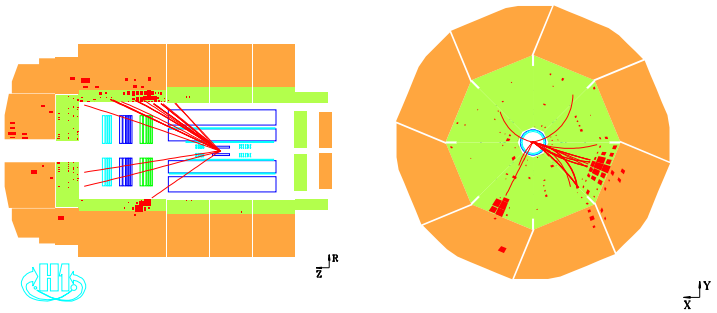

Figure 3.10: *An event with an isolated electron, missing transverse momentum and a prominent hadronic jet observed during the HERA II run 2004.*
The transverse momenta are 37, 44 and 29 GeV/c for the electron, the missing neutrino and the hadronic jet, respectively.

3.6 Progress of Zürich analysis projects

3.6.1 High Q^2 charged current data

In deep–inelastic lepton–proton scattering processes a boson emitted by the lepton interacts with particles inside the proton and causes its dissociation. In the Standard Model of particle physics the interaction can be mediated by four different bosons, namely the electromagnetically interacting photon, γ, and the three weakly interacting bosons, Z_0, and $W^{\pm}$. Two of them, the electrically neutral γ and Z_0, occur in Neutral Current (NC) ep interactions $ep \rightarrow eX$. In NC events the scattered electron and a system of hadrons X form the final state that is observed in the detector. Through the exchange of the charged $W^{\pm}$ boson Charged Current (CC) $ep \rightarrow \nu_e X$ interactions are mediated. The crucial characteristic of CC events is the neutrino, ν_e, in the final state which cannot be detected with the H1 detector. However, the missing transverse momentum can be measured. It is the main observable for the selection of CC events.

An important feature of CC interactions is that they are of weak nature exclusively. The charge of the W boson as well as its sensitivity to the parton helicities make CC interactions particularly well suited to study parton distributions and weak interactions within the Standard Model. The u– and d–quark densities are directly accessible in $e^- p \rightarrow \nu_e X$ and $e^+ p \rightarrow \bar{\nu}_e X$ scattering, respectively. The longitudinally polarised lepton beam which is now available for HERA–II (see Sec. 3.4) provides a new opportunity to test the weak sector of the Standard Model. In CC interactions a positively polarised incoming positron results in a right handed antineutrino. Due to angular momentum conservation the negatively polarised positrons would have to result in left handed anti–neutrinos which do not exist in the Standard Model. Thus, the CC cross section is expected to vanish for negatively polarised positrons. Cross section measurements with longitudinally polarised positrons in combination with the measurement without polarisation could demonstrate the expected linear dependence on polarisation. A measured significant discrepancy from this prediction would be a sign for new physics beyond the Standard Model.

During the upgrade phase for HERA–II a new H1 software environment H1OO based on object oriented programming in C^{++} was designed and implemented. The main goal of this sophisticated change from already established FORTRAN software tools to new software is to provide a modern and extendable framework with standardised physics algorithms that can be incorporated and supported by all H1 physics analyses. The new charged current measurement presented in the recent thesis [44] of Nicole Werner uses this new framework. Another significant change with respect to former measurements is that it is based on reprocessed data, i.e. data with improved track and vertex reconstruction. Figure 3.11 shows the measurement of the single differential charged current

cross section as function of the four momentum transfer squared Q^2. The results are compared to the Standard Model prediction and to the published H1 measurement [3] using the same data sample of 1999/2000 data, corresponding to an integrated luminosity of 65.25 pb^{-1}. The results of both measurements are found to be in good agreement. Due to improvements of the vertex reconstruction and a better simulation of the parton distributions the new result seems to be better described by the Standard Model prediction.
The comparison with the earlier measurement based on the old FORTRAN environment is a vital cross check of whether both analysis frameworks are consistent with each other. Moreover, the development of the programming code for the new measurement was a crucial preparation for the measurement of the charged current cross section with longitudinally polarised leptons. First results of the cross section measurement based on 15.3 pb^{-1} of new HERA–II data with positively polarised positrons are shown in Fig. 3.12 [54]. Despite of its limited statistics the result is in good agreement with the Standard Model prediction. A measurement for negatively polarised positrons is ongoing.

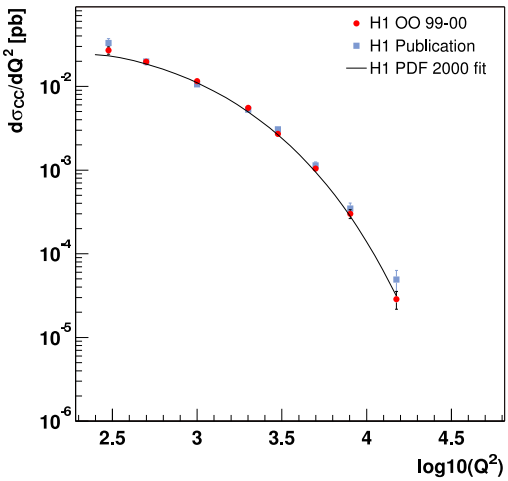

Figure 3.11: *The CC cross section as a function of Q^2. The new measurement based on the new object oriented programming framework (circles) is compared to the H1 publication based on the FORTRAN framework (squares) and to the Standard Model prediction.*

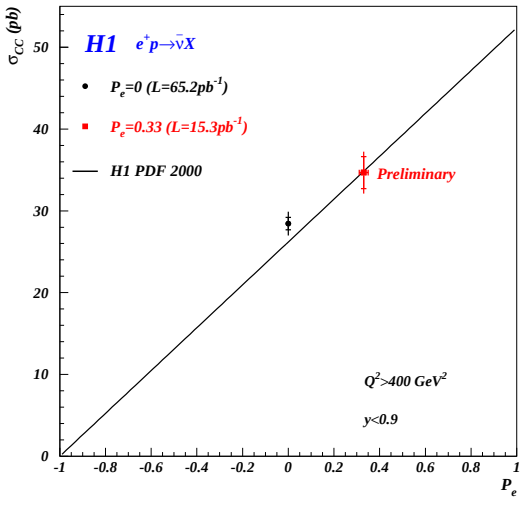

Figure 3.12: *The total CC cross section as a function of longitudinal positron polarisation. Shown are the HERA–I data point without polarisation, the new HERA–II data point measured with positively polarised positrons and the linear curve of the Standard Model prediction.*

3.6.2 Isolated high–p_T τ leptons

Considerable progress has been made this last year in the analysis of isolated, high–p_T τ leptons in events with missing transverse momentum.
Recently Stefania Xella, together with colleagues prepared the first preliminary results for the spring conferences [55]. This analysis is the first H1 analysis on τ leptons and it is a very important parallel result to the previous H1 publications on electron and muon final states where an excess with respect to the total Standard Model expectation was observed at high transverse momentum of the event p_X^T (defined as the total transverse momentum of the event excluding the transverse momentum of the τ candidate).

The current results, for time reasons, are based on a simple τ identification algorithm, exploiting only

one of the various variables which characterise τ jets, namely the jet radius or energy weighted radius of all cells in the τ jet candidate. The final τ identification procedure (to be used for publication later on in the year) will be most probably based on a multi–variable analysis, exploiting fully the different shapes of τ and QCD (background) jets, both longitudinally and transversely, and will provide a better signal over background ratio.

At the current stage of the analysis, H1 does not see any significant excess of data with respect to the Standard Model expectation in the isolated, high–p_T τ lepton analysis, in contrast to what has been seen in the electron and muon channel and in the ZEUS analysis with τ leptons. No events are selected on the 110 pb^{-1} data sample in the region of $p_X^T > 25$ GeV with an expectation of 0.53 events from Standard Model processes. The distribution for the whole p_X^T range is shown in Fig. 3.13 where the number of data selected by all cuts is 5 for a Standard Model expectation of 5.81. In the figure the anomalous top production is also shown scaled to an arbitrary number in order to clearly indicate the region in p_X^T where it would be. Anomalous top production has been considered as one of the possible explanations for the excess at high p_X^T observed in the electron and muon channel. Statistical and systematic errors are currently being investigated, but conservatively should range between 20–30%. This means that the total number of events observed is less than a sigma away from the expectation.

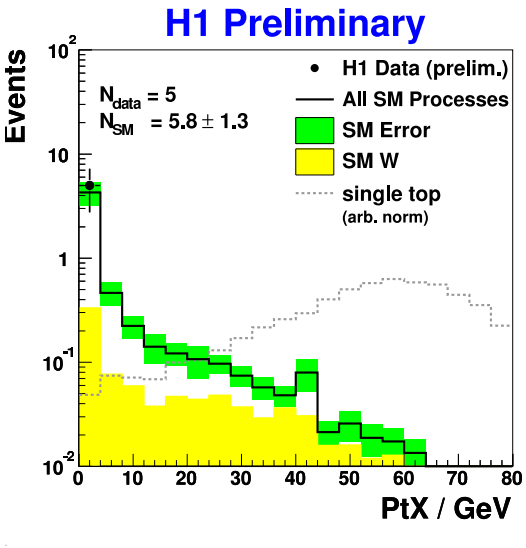

Figure 3.13: *p_X^T of the events selected by the isolated high–p_T τ analysis. In grey is the expected distribution for anomalous top production process, considered as one of the possible interpretations for the excess observed in the electron and muon channel (histogram for top production is scaled to an arbitrary number)*

3.6.3 Prompt photon production

High energy ep collisions at HERA are dominated by electron scattering at small angles with a quasi real photon interacting with the proton (γp collisions). These interactions can also lead to the emission of photons - so called prompt photons - from the hard QCD process, which makes them sensitive both to the partonic structure of the proton and the photon. Though the cross section is very low, this measurement has the advantage that no corrections due to hadronisation or fragmentation processes are necessary.

The prompt photon analysis uses the full integrated luminosity of 133 pb^{-1} from the years 96–00. Prompt photons are identified in the H1 liquid argon calorimeter (LAR) by a compact electromagnetic cluster with transverse energy 5 GeV$< E_T^\gamma <$ 10 GeV in the pseudo–rapidity region $-1 < \eta^\gamma < 0.9$. No track is allowed to point to the candidate. The main experimental difficulty is the separation from hadronic background. The signal from neutral mesons (π^0 or η^0) at high energies is very similar to the signal of a photon since the decay photons cannot be resolved in the calorimeter. The neutral mesons are predominantly produced in jets. Therefore an isolation requirement is applied to the photon

candidate: The transverse energy in a cone of radius one in the (η, ϕ)–plane around the candidate has to be less than $0.1 \cdot E_T^\gamma$. This cut reduces also higher order processes such as events with a photon radiated off the outgoing quark. Events with an identified electron are removed. Furthermore a cut on the inelasticity $y = 1 - E'_e/E_e$ is applied to remove background from DIS events with a badly measured scattered electron. The range of y ($0.2 < y < 0.7$) corresponds to a $\gamma - p$ centre of mass energy of $142 < W < 266$ GeV.

After all selection cuts the background is still of the same size as the signal. The signal is extracted by a detailed analysis of the shower shape.

The results on the inclusive measurement of the prompt photon cross section as a function of transverse energy and pseudo–rapidity were shown at EPS03 [15; 19]. The measurement was now extended to events with an isolated photon and a hadronic jet in the kinematical range $E_T^{jet} > 4.5$ GeV, $-1 < \eta^{jet} < 2.3$. The shape of the inclusive cross section as a function of E_T^γ and η^γ is well described by LO PYTHIA simulation but the MC normalisation is 30% low. The NLO–QCD calculation describes the data well with a tendency to overshoot the data at large η^γ. Cross sections for a prompt photon and a jet are shown in Fig. 3.14 as a function of $E_T^\gamma, \eta^\gamma, E_T^{Jet}, \eta^{Jet}, x_\gamma$ and x_p, the energy fraction, pseudo–rapidity and Bjorken–x of the parton in the proton and the photon, respectively.

The results can be compared with the PYTHIA Monte Carlo and a NLO–QCD calculation. The NLO corrections are significant at low x_p and low x_γ, thus affecting mainly the resolved photon. Multiple interactions are accounted for in NLO calculations by corrections as expected by PYTHIA simulations. The data are well described by the NLO calculation. The results are currently being finalised for publication.

The measurement will be extended into the region of high E_T photons and high η^γ (forward region). At high E_T^γ the photon signal in the calorimeter is hardly distinguishable from the neutral mesons. Therefore the background rejection entirely relies on simulations. This as well as the extension in the forward region requires additional studies on the detector description in the simulation.

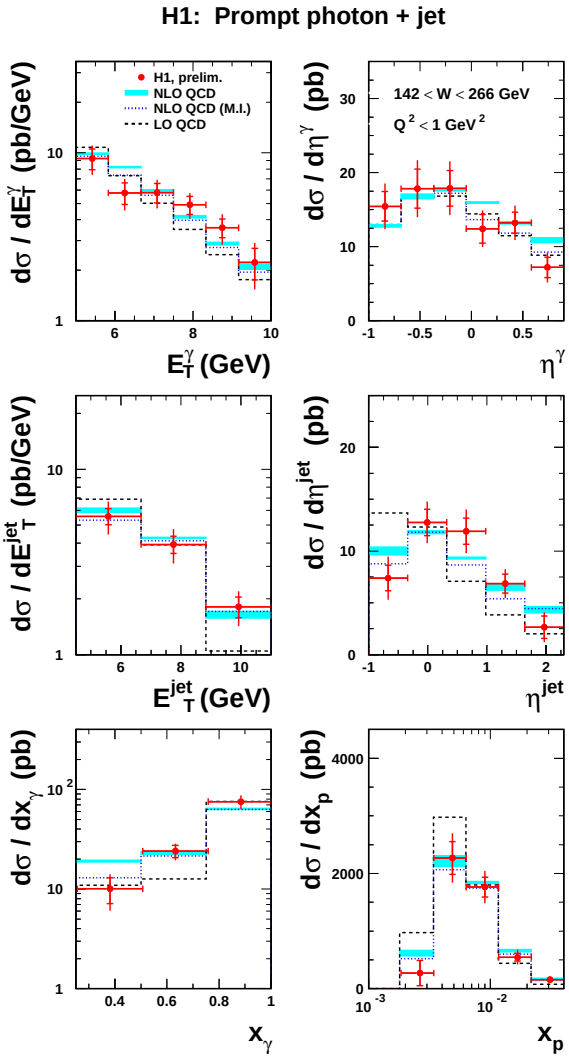

Figure 3.14: *Cross section for prompt photon events with an additional jet as a function of E_T^γ, η^γ, E_T^{Jet}, η^{Jet}, x_γ and x_p. The result is compared to LO Monte Carlo (dashed) and NLO(full) calculation. The dotted line shows the NLO calculation corrected for multiple interactions as determined with PYTHIA simulation.*

A new analysis has started (PhD Thesis Carsten Schmitz) which measures the photon content of jets. The goal is to identify photons inside a hadron jet and measure the photonic energy fraction of the jet. This allows to determine the quark–to–photon fragmentation which is not yet measured in the

kinematic regime of HERA and cannot be estimated by QCD calculations due to its non–perturbative component. The result will be needed for the simulation of physics processes at LHC. The analysis is very challenging because of the photon identification which is hampered by the hadronic environment in the jet and by misidentification of neutral mesons.

3.6.4 QED Compton Scattering

QED Compton events are ep scattering events with a hard photon radiated off the scattered electron. The 4–momentum transfer (Q^2) is very low, hence these events probe the region of very low Q^2 where perturbative QCD models are not valid anymore and phenomenological models have to be tested.

The aim of the analysis is to measure the differential cross section of the QED Compton process. This can be used to determine the structure function F_2 at low Q^2, the transition region between deep–inelastic scattering and real photoproduction, which was so far not accessible with HERA data.

A further motivation is an experimental test of the so called collinear approximation. It is used by several authors to calculate the QED Compton cross section. The approach neglects the transverse momentum of the exchanged photon and treats the photon as a parton of the proton with a structure function describing the photon–parton content of the proton.

- *Event signature:*
  Both the outgoing lepton and the photon are detected in the backward region (wrt the p–beam direction) of the H1 detector almost back–to–back in azimuth. The main difficulty of the analysis is the lepton–photon identification. Roughly 50% of the photons convert before they reach the backward calorimeter (Spacal) and the backward drift chamber (BDC) because all the readout cables and most of the readout electronics of the central tracking chambers are situated in the backward area. The identification of photons and positrons therefore relies on central tracking chambers, namely on the backward silicon detector (BST) in the inner region of the Spacal and the central inner proportional chamber (CIP) in the outer region. The hadronic final state is boosted in the forward direction and can only be measured for inelastic events, which implies that there is no well determined event vertex for most of the events. Therefore a vertex reconstruction using the signals of the scattered lepton in the BST, CIP and BST was used for all events. The analysis is based on a data sample recorded in 1997 with a luminosity of roughly 9 pb^{-1}.

- *Background:*
  Several classes of events can mimic QEDC events, their influence on the cross section measurement was studied. Electron–positron pair production, which is one of the dominant background sources is suppressed by a cut on the total energy in the Spacal and the photon–lepton identification. Photoproduction events with the scattered lepton escaping through the beam–pipe can mimic a QEDC event if several hadronic particles point into the backward region. One of the most significant contributions after the analysis cuts are DIS events with a backward going hadron (typically a π^0) faking a photon. These events were suppressed by a cut on the angular distribution of the hadrons. Deeply virtual Compton scattering, a diffractive process, has the same final state particles as QED Compton scattering and cannot be separated. Its contribution is subtracted, using MC events.

  MC studies showed that the background is well suppressed by the cuts on the total Spacal energy and a maximum angle of clusters in the liquid argon calorimeter. The remaining contribution is estimated by MC studies.

The measurement on the structure function determined with QEDC events was shown at the 2003 conferences [15; 18]. The measurement gives access to the kinematic range down to $Q^2 = 0.1\ GeV^2$ (Fig. 3.15) which was not covered by inclusive measurements at HERA. It is in good agreement with fixed target data.
Nicolas Keller has contributed in his thesis work to this QEDC analysis and recently received his Ph.D. [45].

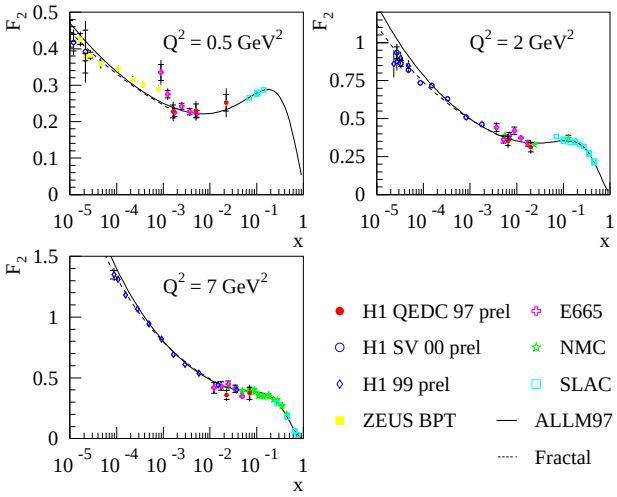

Figure 3.15: *Structure function F_2 as measured with QEDC events for two different Q^2 regions.*

[1] *Isolated Electrons and Muons in Events with Missing Transverse Momentum at HERA*, H1-Coll., V. Andreev *et al.*, DESY 02 – 224, hep-ex/0301030, Phys.Lett.**B561** (2003), 241 - 257.

[2] *Measurement of Inclusive Jet Cross Sections in Photoproduction at HERA*, H1-Coll., C. Adloff *et al.*, DESY 02 – 225, hep-ex/0302034, Eur.Phys.J.**C29** (2003), 497 - 513.

[3] *Measurement and QCD Analysis of Neutral and Charged Current Cross Sections at HERA*, H1-Coll., C. Adloff *et al.*, DESY 03 – 038, hep-ex/0304003, Eur.Phys.J.**C30** (2003), 1 - 32.

[4] *Search for New Physics in $e^{\pm}q$ Contact Interactions*, H1-Coll., C. Adloff *et al.*, DESY 03 – 052, hep-ex/0305015, Phys.Lett.**B568** (2003), 35 - 47.

[5] *Diffractive Photoproduction of J/Ψ Mesons with Large Momentum Transfer at HERA*, H1-Coll., A. Aktas *et al.*, DESY 03 – 061, hep-ex/0306013, Phys.Lett.**B568** (2003), 205 - 218.

[6] *Multi-electron Production at High Transverse Momentum in ep Collisions at HERA*, H1-Coll., A. Aktas *et al.*, DESY 03 – 082, hep-ex/0307015, Eur.Phys.J.**C31** (2003), 17 - 29.

[7] *Search for Single Top Quark Production in $e^{\pm}p$ Collisions at HERA*, H1-Coll., A. Aktas *et al.*, DESY 03 – 132, hep-ex/0310032, Eur.Phys.J.**C33** (2004), 9 - 22.

[8] *Muon Pair Production in ep Collisions at HERA*, H1-Coll., C. Aktas *et al.*, DESY 03 – 159, hep-ex/0311015, Phys.Lett.**B583** (2004), 28 - 40.

[9] *Inclusive Dijet Production at Low Bjorken-x in Deep Inelastic Scattering*, H1-Coll., A. Aktas *et al.*, DESY 03 – 160, hep-ex/0310019, Eur.Phys.J.**C33** (2004), 477 - 493.

[10] *Measurement of Dijet Production at Low Q^2 at HERA*, H1-Coll., A. Aktas *et al.*, DESY 03 – 206, hep-ex/0401010, Eur.Phys.J.**C** (2004), in print.

[11] *Observation of a Narrow Anti-Charmed Baryon State*, H1-Coll., A. Aktas *et al.*, DESY 04 – 038, hep-ex/0403017, Phys.Lett.**B588** (2004), 17.

[12] *Search for Squark Production in R-Parity Violating Supersymmetry at HERA*, H1-Coll., A. Aktas *et al.*, DESY 04 – 025, hep-ex/0403027, Eur.Phys.J.**C** (2004), in print.

[13] *Measurement of Anti-Deuteron Photoproduction and a Search for Heavy Stable Charged Particles in at HERA*, H1-Coll., A. Aktas *et al.*, DESY 04 – 032, hep-ex/0403056, Eur.Phys.J.**C** (2004), in print.

[14] *Forward π^0 Production and Associated Transverse Energy Flow in Deep-Inelastic Scattering at HERA*,
H1-Coll., A. Aktas *et al.*, DESY 04 – 051, hep-ex/0404009, Eur.Phys.J.**C** (2004), in print.

[15] Contributed papers to Int. Europhysics Conf. on High Energy Physics (EPS03), Aachen, Germany (July 2003), and Int. Conf. on Lepton-Photon Interactions (LP03), Fermilab, Chicago, USA (August 2003). Only those papers are listed, which have not yet been submitted to journals; H1-Coll., unless otherwise noted.

[16] *Measurement of the Deep Inelastic Scattering Cross Section at $Q^2 \approx 1$ GeV^2 with the H1 Experiment* (EPS0082, LP165), [15].

[17] *Determination of F_L at Low Q^2* (EPS0083, LP166), [15].

[18] *F_2-measurements at Very Low Q^2 using QED-Compton Events* (EPS0084, LP167), [15].

[19] *Measurement of Prompt Photon Production in γp Interactions* (EPS0093, LP176), [15].

[20] *D^*-μ Correlations in ep Scattering at HERA* (EPS0095, LP177), [15].

[21] *Inclusive D-meson Production in Deep Inelastic Scattering at HERA* (EPS0096, LP178), [15].

[22] *Photoproduction of D^* Mesons at HERA* (EPS0097, LP179), [15].

[23] *D^* Mesons and Associated Jet Production in Deep Inelastic Scattering* (EPS0098, LP180), [15].

[24] *Forward Jet Production at HERA* (EPS0109, LP189), [15].

[25] *Two-Jet and Three-Jet Differential Event Shapes in Deep Inelastic Scattering* (EPS0111, LP191), [15].

[26] *Measurements of Beauty Production using Semi-muonic Decays* (EPS0117, LP194), [15].

[27] *Diffractive Photoproduction of Jets at HERA* (EPS0087, LP170), [15].

[28] *Measurement of the Diffractive DIS Cross Section at low Q^2* (EPS0088, LP171), [15].

[29] *Measurement and NLO DGLAP QCD Interpretation of Diffractive Deep Inelastic Scattering at HERA* (EPS0089, LP172), [15].

[30] *Measurement of the Inclusive Diffractive Cross Section $\sigma_r^D(3)$ at high Q^2* (EPS0090, LP173), [15].

[31] *Diffractive Dissociation in Photoproduction at HERA* (EPS0091, LP174), [15].

[32] *Elastic Electroproduction of ρ-mesons at High Q^2* (EPS0092, LP175), [15].

[33] *Inclusive ρ, $f_0(980)$, $f_2(1270)$, and η Photoproduction* (EPS0107, LP187), [15].

[34] *Elastic Photoproduction of J/ψ Mesons* (EPS0108, LP188), [15].

[35] *Diffractive Photoproduction of High p_t Photons at HERA* (EPS0110, LP190), [15].

[36] *Comparison at NLO between Diffractive Final State Observables and Predictions from Fits to F_2^D* (EPS0113, LP192), [15].

[37] *Deeply Virtual Compton Scattering Cross Section Measurement at Medium and Small Photon Virtualities* (EPS0115, LP193), [15].

[38] *Search for Doubly Charged Higgs Production at HERA* (EPS0104, LP184), [15].

[39] *A Search for Leptoquarks at HERA* (EPS0105, LP185), [15].

[40] *A Search for Magnetic Monopoles at HERA* (EPS0106, LP186), [15].

[41] *General Search for New Phenomena at HERA* (EPS0118, LP195), [15].

[42] *Search for Superlight Gravitinos at HERA* (LP196), [15].

[43] *A New z–Vertex Trigger for H1*, Max Urban, PhD Thesis, University of Zürich (2004).

[44] *Measurement of the Charged Current Cross Section in Positron–Proton Scattering at HERA*, Nicole Werner, PhD Thesis, University of Zürich (2004).

[45] *A Measurement of the QED Compton Cross Section in Electron-Proton Scattering with the H1*

Experiment at HERA,
N. Keller, PhD Thesis, University of Zürich (2003).

[46] *A New Analysis for the Transverse Polarimeter at HERA II*,
T. Behnke, J. Böhme, B. List, and S. Schmitt (EPS0120), [15].

[47] S. Aid *et al.*, H1-Coll., Nucl. Phys. **B472** (1996), 32; C. Adloff *et al.*, H1-Coll., Nucl. Phys. **B545** (1999), 21; C. Adloff *et al.*, H1-Coll., Phys.Lett.**B528** (2002), 199.

[48] *High P_T analysis of HERA II data*, H1-report H1prelim-04-063, see [52] .

[49] *A Measurement of Beauty Production in High-Energy Positron-Proton Scattering*,
J. Kroseberg, PhD thesis, University of Zürich (2003).

[50] *Measurement of Beauty Production in Deep Inelastic scattering at HERA*,
H1-report H1prelim-04-071, see [52].

[51] *Measurement of $F_2^{c\bar{c}}$ and $F_2^{b\bar{b}}$ at High Q^2*,
H1-report H1prelim-04-072, see [52].

[52] available at http://www-h1.desy.de/publications/H1preliminary.short_list.html.

[53] B.W. Harris, and J. Smith, Nucl. Phys. **B452** (1995), 109.

[54] *Measurement of Polarised Charged Current Total Cross Section at HERA II*,
H1-report H1prelim-04-041, see [52].

[55] *Search for Events with τ-leptons in ep Collisions at HERA*,
H1-report H1prelim-04-061, see [52].